Simulation Study of Dielectron Production in Bi+Bi Collisions at $\sqrt{s_{\rm NN}} = 9.2$ GeV at NICA-MPD

Yonghong Wang[a,b]

Chi Yang[a,1]

[a] Key Laboratory of Particle Physics and Particle Irradiation (MOE), Institute of Frontier and Interdisciplinary Science, Shandong University

[b] Veksler and Baldin Laboratory of High Energy Physics, Joint Institute for Nuclear Research

The Multi-Purpose Detector (MPD) at the NICA facility is designed to study heavy-ion collisions at $\sqrt{s_{\rm NN}}$= 4–11 GeV, aiming to explore the baryon-rich region of the QCD phase diagram to investigate the possible existence of a first-order phase transition and a critical end-point (CEP). Dileptons, serving as a key electromagnetic probe, are sensitive to the temperature, lifetime, and total baryon density of the hot, dense medium. The measurement of dielectrons is treated as an effective way to search for the QCD phase structure, chiral symmetry restoration, and possible CEP related phenomena.

We present a feasibility study of dielectron production in Bi+Bi collisions at $\sqrt{s_{\rm NN}}$= 9.2 GeV using full MPD detector simulations with realistic event generators. Details are provided on electron reconstruction using the Time Projection Chamber (TPC), Time-of-Flight (TOF) detector, and Electromagnetic Calorimeter (ECal), background suppression techniques for photon conversions and π^0 Dalitz decays, and performance evaluation based on signal-to-background ratio (S/B) and statistical significance (n_σ). These established reconstruction and background suppression procedures provide support for future experimental data analysis, and the results verify the ability of MPD to perform high-precision dielectron measurements.

PACS: 25.75.Nq; 25.75.Cj; 29.40.Gx; 24.10.Lx

Introduction

The quark–gluon plasma (QGP) is a strongly interacting deconfined state of matter that is believed to have existed in the early universe, a few microseconds after the Big Bang [1]. Experimentally, heavy-ion collisions make it possible to create and study strongly interacting matter under extreme conditions in the laboratory [2]. A central challenge in this field is to determine the nature of the phase transition between QGP and hadronic matter—whether it is a first-order phase transition or a smooth crossover. Within the framework of quantum chromodynamics (QCD), such a transition is expected to occur as a function of temperature and baryon chemical potential [3]. The corresponding QCD phase diagram is shown in the left panel of Fig. 1. The Nuclotron-based Ion Collider fAcility (NICA) in Dubna, along with its Multi-Purpose Detector (MPD) experiment (middle panel of Fig. 1), is designed

[1]E-mail: chiyang@sdu.edu.cn

to address this challenge by exploring the high-baryon-density region of the QCD phase diagram [4]. This will be achieved through heavy-ion collisions at $\sqrt{s_{\rm NN}}$= 4 - 11 GeV, a regime predicted to be favorable for discovering a first-order phase transition [4]. The MPD physics program relies on the capabilities of several key MPD subsystems. The TPC provides the primary functions of three-dimensional charged-particle tracking, momentum measurement, and particle identification via energy loss (dE/dx) [5]. The TOF system improves particle identification by providing velocity measurements and consists of 28 modules equipped with Multi-gap Resistive Plate Chambers (MRPCs) [6]. The ECal is designed to measure the energy and position of electrons and photons and plays a key role in electromagnetic probe measurements [7].

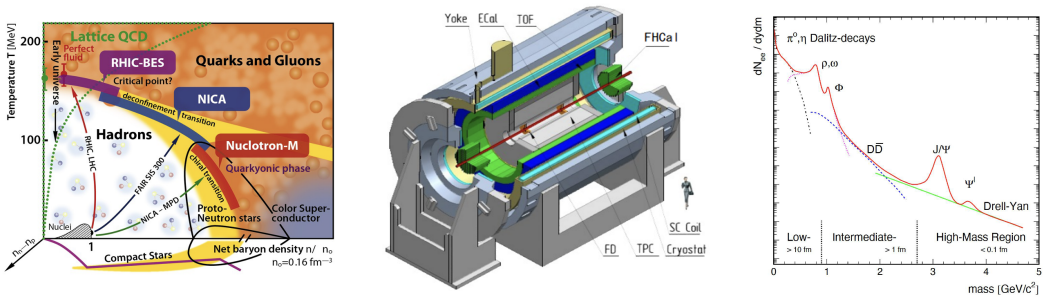


Fig. 1: Left: The phase diagram of QCD, illustrating the transition from hadronic matter to QGP at high temperatures and baryon densities. Middle: The layout of MPD detector. Right: Expected sources for dielectron production as a function of invariant mass in ultra-relativistic heavy-ion collisions [8].

Dielectrons are electromagnetic probes for studying the QGP. Their importance stems from fundamental properties: they are emitted from the early to final stages of the collision, do not interact with the strongly interacting matter, and have a mean free path that significantly exceeds the system size. These characteristics enable them to convey information from their point of origin without distortion. In contrast to direct photons, dielectrons are not affected by blue-shift effects from collective radial flow, and their invariant mass spectrum ((Fig. 1) [8]) can be decomposed into contributions from distinct production sources, thereby providing a tomographic probe of the collision. In the high-mass region ($M_{ee} > 3$ GeV/c^2), the spectrum is dominated by Drell–Yan processes and decays of heavy quarkonia [8]. The intermediate-mass region ($1 < M_{ee} < 3$ GeV/c^2) contains contributions from thermal radiation emitted by the QGP as well as semi-leptonic decays of correlated charm–anticharm pairs. In the low-mass region ($M_{ee} < 1$ GeV/c^2), the spectrum is primarily governed by dielectron decays of light vector mesons with in-medium line shape modifications [9]. The principal application of dielectrons lies in their dual role as a thermometer and a chronometer. The spectral shape in the intermediate-mass region is directly sensitive to the ini-

tial temperature of the QGP, while the preservation of the total yield from the moment of electromagnetic emission allows for an estimation of the system's lifetime, making it a unique probe for quantifying key QGP properties.

This analysis utilizes a data set of 15 million Bi+Bi collisions at $\sqrt{s_{\rm NN}}$= 9.2 GeV, generated with the Ultra-relativistic Quantum Molecular Dynamics Model (UrQMD) event generator [10]. The simulated dielectron signals were corrected to comply with those predicted by the Parton-Hadron-String Dynamics(PHSD) [11], while the underlying background contributions were estimated by UrQMD. The PHSD event generator proved to be very successful in description of dielectron spectra measured by STAR experiment in Au+Au collisions in a wide energy range $\sqrt{s_{\rm NN}}$= 7.7-200 GeV [12].

Electron identification

Event selection requires a reconstructed primary vertex position within ±80 cm along the beam axis, leaving 11 million events to be analyzed. Electron candidates were selected based on the track quality and particle identification selections. Tracks were required to have at least 39 hits in the TPC, a rapidity $|\eta| < 1$, a distance of closest approach to the primary vertex within 2.5σ, and a minimum transverse momentum of 200 MeV/c. Additionally, selected tracks were required to be matched to the TOF within 3σ in dϕ and 2σ in dZed.

Electron identification (eID) was performed using a combination of the TOF and TPC. The TOF selection requires the measured β value to lie within 2σ of the expectation for electrons, as shown in the top-middle panel of Fig. 2. The subsequent dE/dx distribution obtained from TPC, expressed in terms of sigma deviations from the electron expectation (top-left panel of Fig. 2), exhibits a prominent electron peak at zero with significant pion contamination. A 2σ exclusion cut was applied to pions to enhance electron purity. A momentum-dependent eID cut (dashed line in the top-left panel) was further employed to improve pion–electron separation. The ECal was also evaluated for eID. Tracks were matched to the ECal within 2σ. Two discriminating variables were considered: the time-of-flight converted to m^2, and the energy-to-momentum ratio E/p. The ECal time resolution was simulated equal to 500 ps, which limits its identification capability to very low-$p_{\rm T}$ electrons and offers limited hadron rejection. The E/p ratio for electrons is expected to be close to unity. The red lines in the bottom panels of Fig. 2 indicate the adopted selection criteria.

The right panel of Fig. 2 summarizes the electron purity and reconstruction efficiency for different identification strategies. Using TPC and TOF for eID yields an electron efficiency of $\sim$ 50% and a purity exceeding 60% across a broad momentum range. When ECal selections are included, the efficiency decreases to about 45%, while the purity approaches nearly 100%.

Invariant mass of dielectrons

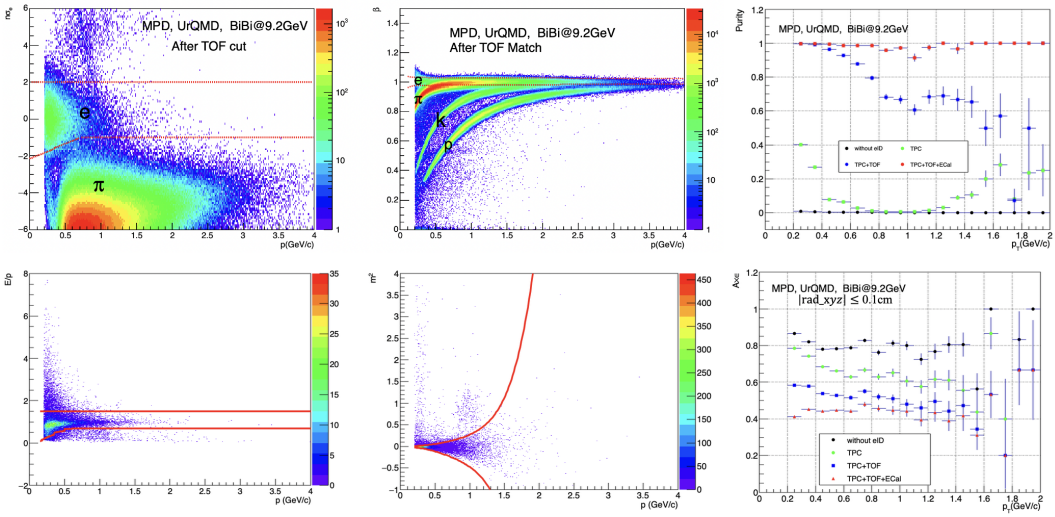


Fig. 2: Electron identification strategies and performance in minimum-bias Bi+Bi collisions at $\sqrt{s_{NN}} = 9.2$ GeV. The top-left panel shows the n_{σ_e} distribution for TOF-matched tracks with the TOF cut $|\sigma_{\beta_e}| < 2$, where the TPC eID selection is indicated by the red lines. The top-middle panel presents the TOF β distribution, where the TOF eID cut $|\sigma_{\beta_e}| < 2$ is indicated by the red lines. The bottom-left and bottom-middle panels show the ECal E/p and squared mass m^2 distributions, respectively, with electron selections marked by red lines. The top-right and bottom-right panels display the resulting electron purity and reconstruction efficiency for different identification strategies.

Following the selection of electron candidates using the TPC and TOF detectors, the resulting invariant mass distribution of pairs is displayed with black markers in the top panel of Fig.3. The distribution in pink represents pairs where both particles are confirmed as true electrons or positrons based on Monte Carlo (MC) information, indicating that the majority of the collected pairs are true dielectrons. However, significant hadronic contamination is observed at invariant masses above 0.6 GeV/c^2. The blue curve depicts the signal of interest. The red and green distributions correspond to pairs in which the electron and/or positron originates from photon conversions (PCM) or π^0 Dalitz decays, which are identified as the two dominant background contributions.

The black and blue dots in the left panel of Fig. 3 are the same as those in the top panel. The green curve corresponds to the background estimated using the like-sign method. The right panel presents the final invariant mass distribution after background subtraction. Despite the high purity of single-electron identification, the signal-to-background ratio (S/B) integrated over the mass range of 0.2–1.5 GeV/c^2 is only 1.2% due to the overwhelming combinatorial background. The corresponding signal significance ($S/\sqrt{B}$) is 6.6σ. In dielectron measurements, maintaining a high signal significance is essential for the statistical observation of the signal, while a favorable S/B ratio is crucial for minimizing systematic uncertainties associated with

background subtraction. To improve this, a more effective rejection of background pairs is required. Consequently, developing a robust method to tag and reject electrons from photon conversion and Dalitz decays is expected to significantly enhance both the S/B ratio and the signal significance.

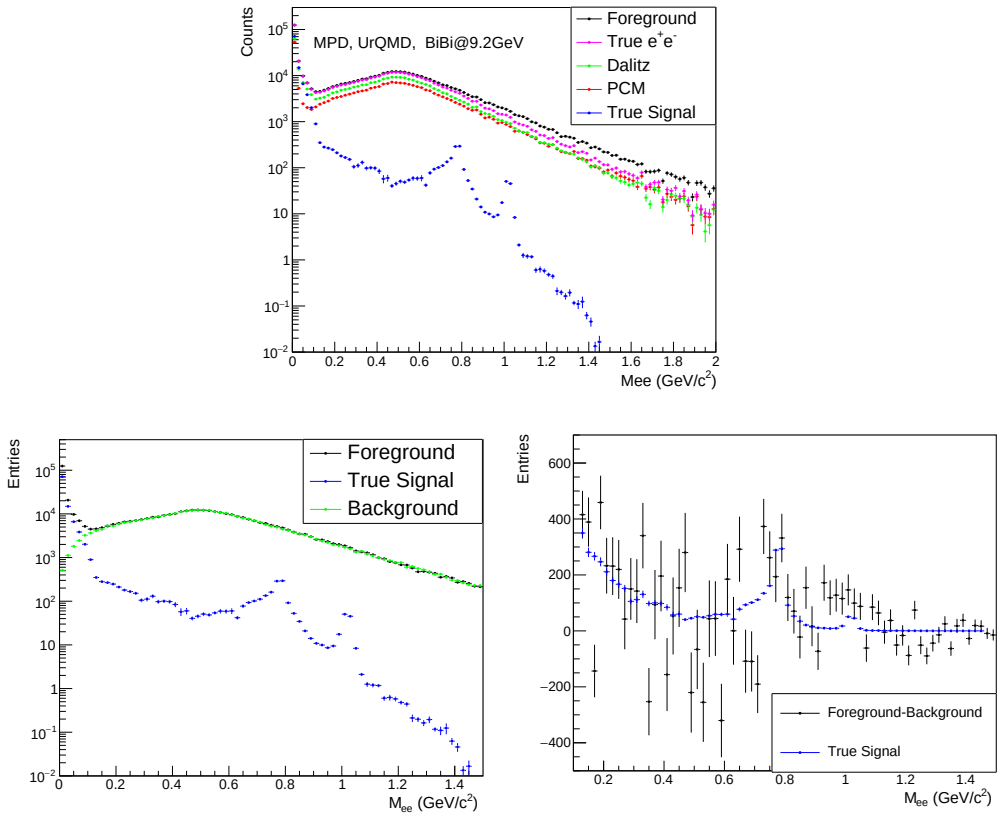


Fig. 3: Top: invariant mass distribution of e^+e^- pairs from different sources after TPC+TOF eID cut. Left: the total distribution (black), the true signal (blue) and the background estimated by like-sign method (green). Right: the comparison of the final spectrum after background subtraction and true signal.

Tagging and rejection electron from PCM

A procedure was developed to tag and reject electrons and positrons originating from photon conversions to reduce background. The photon conversion mostly happens in the detector materials and the produced e^+e^- pairs can be identified based on their specific production geometry with the production vertices shifted from the primary vertex. In this method, all tightly (as defined in the previous section) identified e^+/e^- are combined with oppositely charged e^-/e^+ candidates in the same event. These partner tracks are required to have at least 10 hits in the TPC, a rapidity $|\eta| < 2.5$, and to be identified with $|n\sigma_e|<2$ using the TPC alone, or $|n\sigma_e|<2$ and $|\sigma_{\beta_e}| < 2$

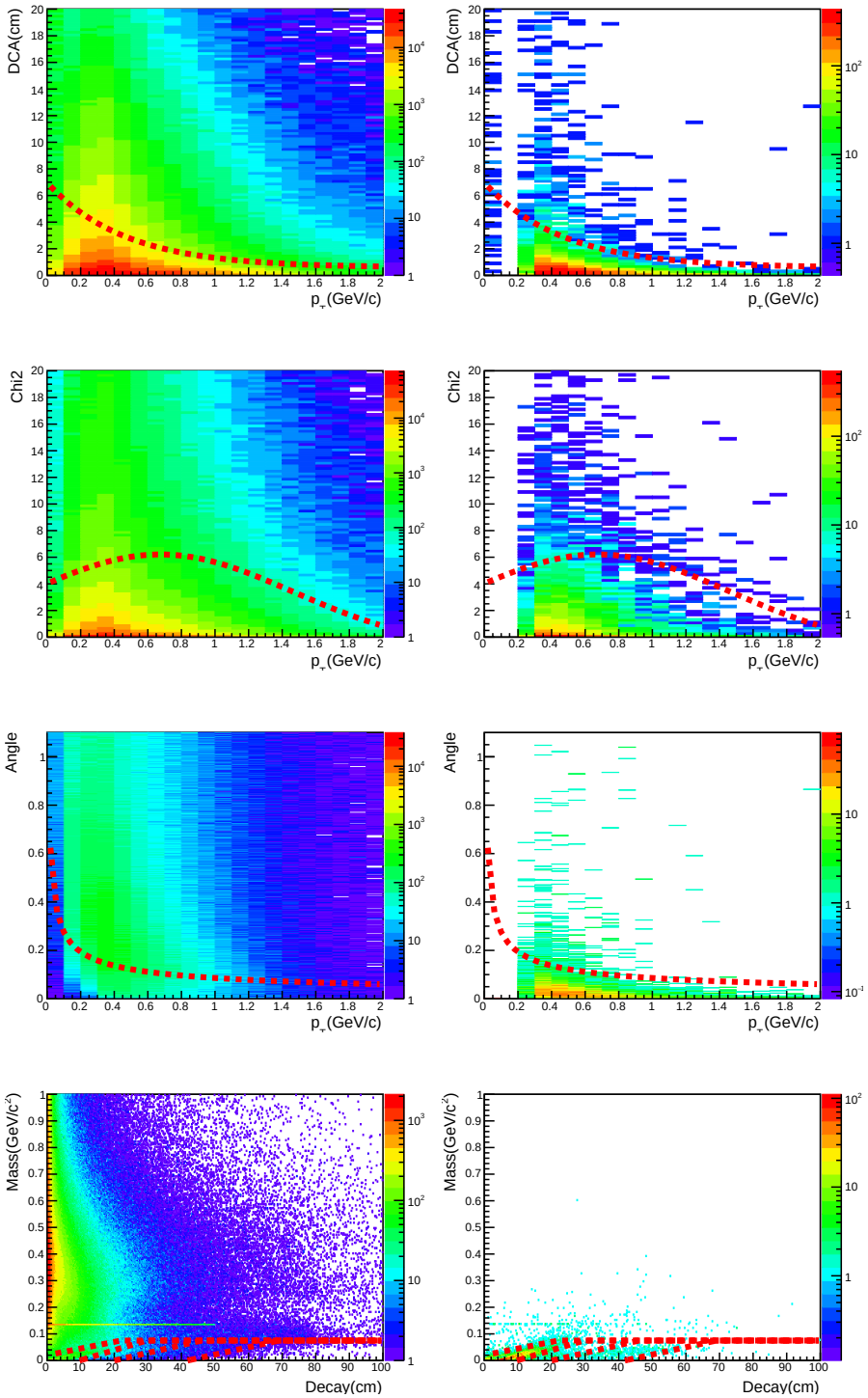


Fig. 4: Tagging e^+/e^- from photon conversions. Distributions of pair variables for all combinations (left column) and for true photon conversions (right column). The red lines indicate the applied cuts to tag and reject e^+/e^- from photon conversions.

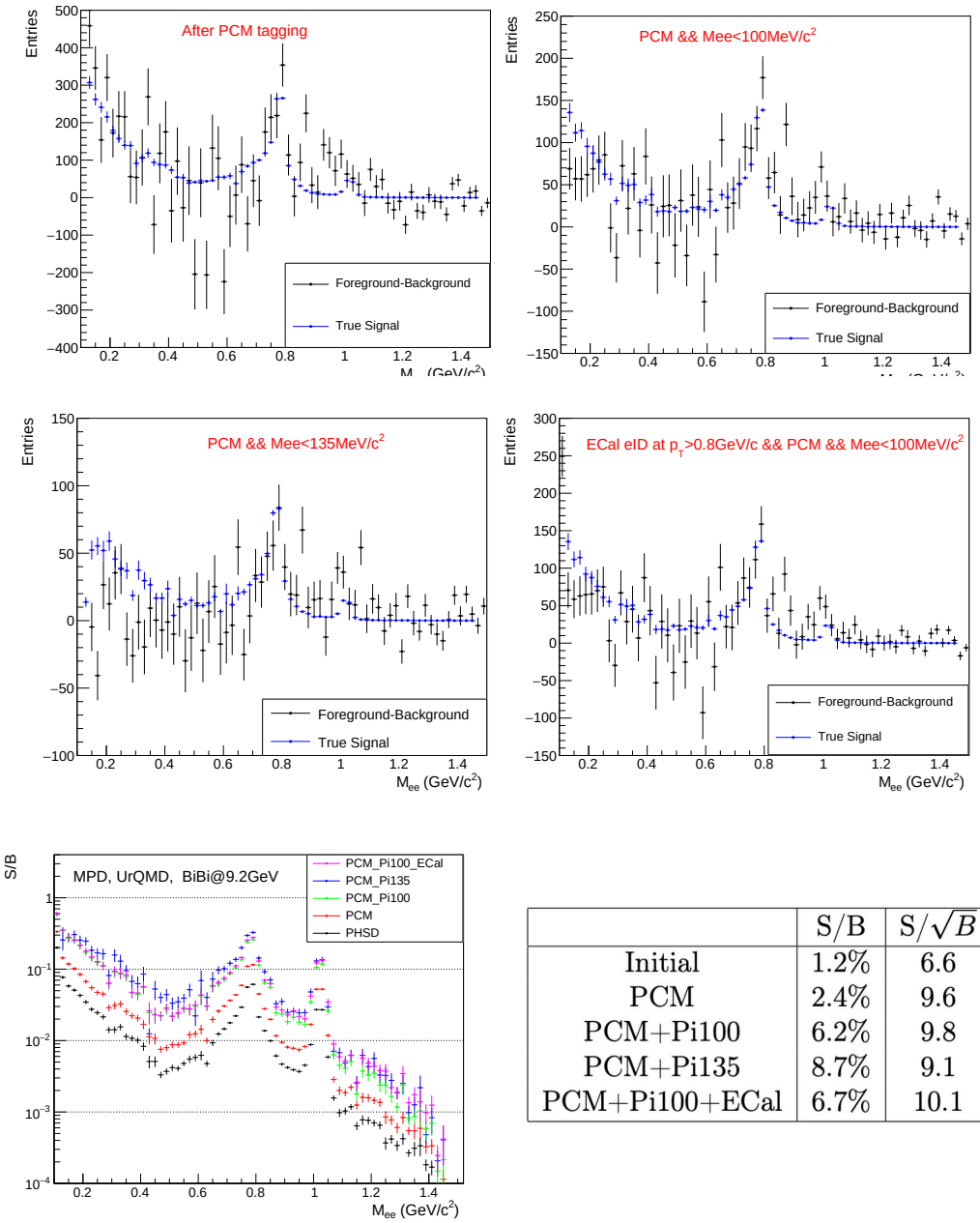
using both the TPC and TOF if partner tracks are additionally matched to the TOF. Photon conversion pairs are identified using several discriminating variables: the Distance of Closest Approach (DCA) between the two tracks at the secondary vertex, the χ^2/NDF of the quality of the secondary vertex reconstruction, the pointing angle of the pair to the primary vertex, and the dependence of the reconstructed pair mass on the decay length. The distributions of these variables are presented in Fig.4: the left line shows all paired combinations, while the right line shows pairs that are from true photon conversions. The dashed curves in the panels represent the selection criteria applied to tag conversion pairs. With these cuts, approximately 80% of the true photon conversion pairs are successfully identified for rejection.

Following the tagging and removal of photon conversion electrons, the comparison between the reconstructed invariant mass distribution after background subtraction and the true reconstructed signal is shown in the top-left panel of Fig.5. An improvement in the agreement between the reconstructed (black) and true signal (blue) distributions is observed after PCM rejection. This qualitative improvement is quantitatively confirmed by the S/B, which increases by approximately a factor of two. Correspondingly, $S/\sqrt{B}$ improves by about 50%. Despite this noticeable progress, the overall background level remains substantial, indicating that further background suppression strategies are necessary.

Tagging and rejection electron from Dalitz decay

To further suppress the background, a procedure was developed to tag electrons and positrons originating from π^0 Dalitz decays. The methodology is analogous to that used for photon conversion tagging: all tightly (as defined in the previous section) identified e^+/e^- are combined with oppositely charged e^-/e^+ candidates in the same event. The selection criteria for these partner tracks are largely consistent with those applied in the PCM rejection. Specific to Dalitz decay tagging, two additional requirements are imposed. First, given that the decay vertices of Dalitz pairs are typically indistinguishable from the primary vertex, tracks of partners are required to be matched to the primary vertex within 5σ. Second, the invariant mass of the pair must lie below a predefined upper limit; an initial mass cut of 100 MeV/c^2 was applied (Pi100). A S/B of 6.2% and a $S/\sqrt{B}$ of 9.8σ are achieved. Both of these criteria are subjects for further optimization to maximize background rejection.

In the special case, relaxing this Dalitz mass cut from 100 to 135 MeV/c^2 (Pi135) increases the S/B from 6.2% to 8.7%. This improvement in purity, however, is achieved at the expense of a reduced $S/\sqrt{B}$, which decreases from 9.8σ to 9.1σ. Separately, the analysis was performed with an additional eID requirement based on the ECal for tracks with $p_{\mathrm{T}} > 0.8$ GeV/c. Under this condition, and with all other background rejection methods applied, a S/B of 6.7% and a $S/\sqrt{B}$ of 10.1σ are achieved. The background-subtracted dielectron invariant mass spectrum and the true reconstructed signal for different



	S/B	$S/\sqrt{B}$
Initial	1.2%	6.6
PCM	2.4%	9.6
PCM+Pi100	6.2%	9.8
PCM+Pi135	8.7%	9.1
PCM+Pi100+ECal	6.7%	10.1

Fig. 5: Progression of background suppression strategies and their performance. The four panels on the top and center compare the dielectrons invariant mass spectra after background subtraction under different track selections

to the true signal. Top-left: PCM rejection, top-right: Dalitz rejection at mass < 100 MeV/c^2, middle-left: Dalitz rejection at mass < 135 MeV/c^2, and middle-right: further applying an ECal eID cut at $p_{\mathrm{T}} > 0.8$ GeV/c. The bottom panels provide a quantitative assessment, showing the S/B (left), S/B and $S/\sqrt{B}$ values (right) for each strategy.

background suppression strategies are shown in Fig.5. The corresponding S/B and $S/\sqrt{B}$ for each strategy are summarized in the table.

Conclusion

Dielectron measurements constitute an important part of the physics program of the MPD experiment, providing a sensitive probe of strongly interacting matter created in heavy-ion collisions. As the MPD experiment approaches full integration, simulation studies are essential for evaluating the feasibility of dielectron measurements and developing robust analysis strategies. A comprehensive simulation study based on the UrQMD event generator for Bi+Bi collisions at $\sqrt{s_{\mathrm{NN}}} = 9.2$ GeV with 15 million events was performed to assess the expected performance of the MPD detector. The results show that an electron purity of about 100% and a reconstruction efficiency of approximately 45% can be achieved at $p_{\mathrm{T}} > 200$ MeV/c using combined TPC, TOF and ECal electron identification. Despite the relatively high electron purity using TPC+TOF eID, the dielectron invariant mass spectrum remains dominated by a large combinatorial background, mainly from photon conversions and Dalitz decays of light neutral mesons, highlighting the need for dedicated background suppression methods. To address this, a tight–loose tagging algorithm was developed and tested within the simulation framework. This method significantly enhances the measurement performance, increasing the S/B from 0.2% to 6.7% and improving the $S/\sqrt{B}$ from 6.6σ to 10.1σ in the mass range of 0.2–1.5 GeV/c^2. These results demonstrate the feasibility of dielectron measurements at MPD and suggest that the first meaningful results can be achieved with an accumulation of 100+ million events. Furthermore, this study provides a solid reference for optimizing electron and pair selection criteria and background suppression techniques.

FUNDING

This work was supported by the Shandong Provincial Natural Science Foundation (Project No. ZR2022JQ03) and by the Program of the China Scholarship Council (Project No. 202306220145).

CONFLICT OF INTEREST

The authors of this work declare that they have no conflicts of interest.

Acknowledgements

The author thanks the MPD Collaboration for their guidance.

REFERENCES

1. *Mustafa M.G.* Quark–Gluon plasma and heavy-ion phenomenology // The European Physical Journal Special Topics. 2021. V. 230, no. 3. P. 603–605.

2. *Foka P., Janik M.A.* An overview of experimental results from ultra-relativistic heavy-ion collisions at the CERN LHC: Bulk properties and dynamical evolution // Reviews in Physics. 2016. V. 1. P. 154–171. URL: https://www.sciencedirect.com/science/article/pii/S2405428316300156.

3. *Zhu X., Yong G.C.* Exploring hadron-quark phase transition in heavy-ion collisions using particle emission ratios in heavy and light reaction systems // Phys. Lett. B. 2025. V. 865. P. 139454. arXiv:2411.13110.

4. *Collaboration M.* MPD physics performance studies in Bi+Bi collisions at $\sqrt{s_{NN}} = 9.2$ GeV. 2025. arXiv:2503.21117.

5. *Abgaryan V. et al.* [MPD Collaboration] Status and initial physics performance studies of the MPD experiment at NICA // Eur. Phys. J. A. 2022. V. 58, no. 7. P. 140. arXiv:2202.08970.

6. *Baryshnikov V., others.* Status of the Time-of-Flight and ECal Particle Identification Systems of the MPD Experiment at the NICA Collider // Moscow Univ. Phys. Bull. 2024. V. 79, no. Suppl 1. P. 33–38.

7. *Wang Y., Hu K., Yang C.* Fabrications and Performance Test of ECal Modules in China for NICA-MPD Experiment // Moscow Univ. Phys. Bull. 2024. V. 79, no. Suppl 1. P. 42–45.

8. *Rapp R., Wambach J.* Chiral symmetry restoration and dileptons in relativistic heavy ion collisions // Adv. Nucl. Phys. 2000. V. 25. P. 1. arXiv:hep-ph/9909229.

9. *Jin C. et al.* [STAR Collaboration] Dielectron measurements in Au+Au collisions at BES-II energies with the STAR experiment. 2025. 5. arXiv:2505.06361.

10. *Bleicher M., others.* Relativistic hadron hadron collisions in the ultrarelativistic quantum molecular dynamics model // J. Phys. G. 1999. V. 25. P. 1859–1896. arXiv:hep-ph/9909407.

11. *Bratkovskaya E.L., Cassing W., Konchakovski V.P., Linnyk O.* Parton-Hadron-String Dynamics at Relativistic Collider Energies // Nucl. Phys. A. 2011. V. 856. P. 162–182. arXiv:1101.5793 [nucl-th].

12. *Jorge A.W.R., Song T., Zhou Q., Bratkovskaya E.* Electromagnetic emission from strongly interacting hadronic and partonic matter created in heavy-ion collisions // Phys. Rev. C. 2025. V. 111, no. 6. P. 064904. arXiv:2503.05253.